

GT2011-4636&

EXPERIMENTAL INVESTIGATION ON LEAKAGE LOSSES AND HEAT TRANSFER IN A NON CONVENTIONAL LABYRINTH SEAL

Luca Bozzi, Enrico D'Angelo
Ansaldo Energia S.p.A.
Product Development/ Turbomachinery
Via Lorenzi 8, 16162
Genoa (Italy)
Luca.Bozzi@aen.ansaldo.it

Bruno Facchini, Mirko Micio, Riccardo Da Soghe
Department of Energy "Sergio Stecco"
University of Florence
Via Santa Marta 3
50139 Florence (Italy)
mirko.micio@htc.de.unifi.it

ABSTRACT

Different labyrinth seal configurations are used in modern heavy-duty gas turbine such as see-through stepped or honeycomb seals. The characterization of leakage flow through the seals is one of the main tasks for secondary air system designers as well as the evaluation of increase in temperature due to heat transfer and windage effects. In high temperature turbomachinery applications, knowledge of the heat transfer characteristics of flow leaking through the seals is needed in order to accurately predict seal dimensions and performance as affected by thermal expansion.

This paper deals with the influence of clearance on the leakage flow and heat transfer coefficient of a contactless labyrinth seal. A scaled-up planar model of the seal mounted in the inner shrouded vane of the Ansaldo AE94.3A gas turbine has been experimentally investigated. Five clearances were tested using a stationary test rig. The experiments covered a range of Reynolds numbers between 5000 and 40000 and pressure ratios between 1 and 3.3.

Local heat transfer coefficients were calculated using a transient technique. It is shown that the clearance/pitch ratio has a significant effect upon both leakage loss and heat transfer coefficient. Hodkinson's and Vermes' models are used to fit experimental mass flow rate and pressure drop data. This approach shows a good agreement with experimental data.

1. INTRODUCTION

Despite advanced techniques such as gas-film seals, labyrinth seals remain the most important and widely used sealing elements in turbomachinery, due to their reliability.

Because of their simplicity, straight through labyrinths are mainly selected especially where small seal gaps can be realized. In areas where superior sealing is required, as at the exit of high-pressure compressors with larger diameters and hence larger clearances, stepped labyrinth seals are preferred.

The main tasks of this contactless seal are to reduce the unwanted leakage between the rotating and stationary components of the engine and to control the cooling air supply. A small clearance accommodates the differential thermal expansion between the rotating fins and the shroud as well as the centrifugal growth. Although this clearance allows parasitic losses, it guarantees a high durability of the seal.

The design of a labyrinth is almost always a compromise between the desire to get the greatest number of throttling in a given space or per unit length and, at the same time, to leave the pitch distance between the restrictors large enough to reduce to a minimum the carry-over of kinetic energy from one throttling to the next. Since these two criteria are contradictory, the designer is faced with a problem. Because certain features of the labyrinth's behaviour can not yet be reliably predicted, a general analytical means by which such an optimum could be obtained does not exist, even for the simplest labyrinth configurations.

Labyrinth seal leakage is primarily dependent on clearance, number of seal fins, over-all pressure ratio, and the inlet pressure and temperature of the fluid. The actual design of seals depends primarily on two geometric parameters: the shape of teeth and the size and shape of the chamber between teeth. The influence of the tooth shape results from the following factors: the tooth tip-width to clearance ratio and the angle that the front face of the tooth makes with the flow.

The size and shape of the chambers between the teeth affects the strength of eddies and vortices formed there, and they in turn control the conversion of kinetic energy to thermal energy. Apparently the depth of the teeth does not have as great an effect on limiting the leakage as does the pitch.

Flow visualization and experimentation by Jerie [11] indicates that the optimum tooth depth is equal to or

slightly less than the pitch. In fact, the data obtained by Jerie shows that if the teeth are too closely spaced, the resultant leakage can be larger than that passed by a single tooth.

Leakage prediction is based upon the principle of a number of restrictions in series. Since the dissipation of the jet is not 100 percent efficient, Egli (1935) introduced the concept of the carry over factor [2]. Usually engine companies have considerable experience with labyrinth seals and they use their own empirical corrections to Egli's formula.

Few publications dealing with the heat transfer in labyrinth seals are available in literature and only a small part provides more detailed investigations of the distribution of the local heat transfer coefficients like Metzger et al. [20] and Willenborg et al. [21], [22].

Most studies are based on the assumption that there is only a negligible effect of rotation on the leakage rate and heat transfer in labyrinth seals. Becker (1907) found no rotational effects on the labyrinth flow. Friedrich (1933) measured a 20% leakage reduction in a rotating straight-through labyrinth seal and Yamada (1962) observed a maximum increase of the drag coefficient by a factor 10, if the flow was laminar, but rotation had little impact on the seal flow as soon as the flow becomes turbulent [1].

From Waschka et al. (1991) [1] it can be seen that for ratio $Ta/Re < 0.2$ the influence of rotation on through flow is negligible. The studies have also demonstrated that rotation cannot be neglected at small axial Reynolds number and high Taylor numbers.

1.1 Ansaldo sealing system of AE94.3A GT

Figure 1 illustrates the AEN seal geometry nomenclature.

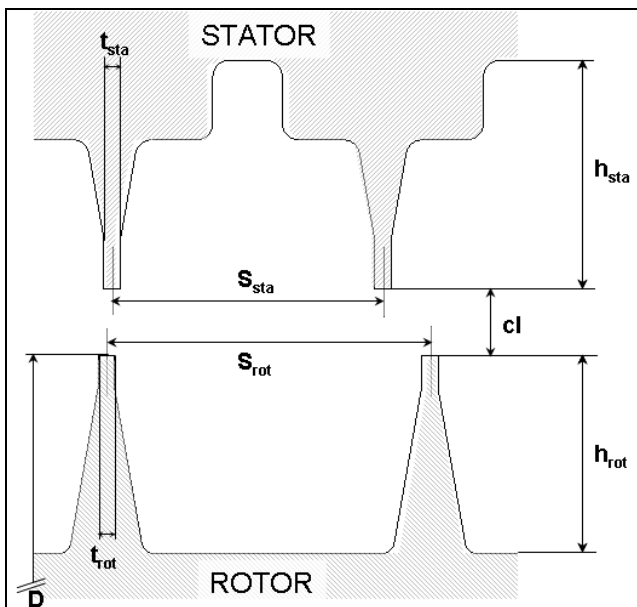


Fig. 1: studied configuration for labyrinth seal

- Number of Teeth, N.

It is the number of teeth or blades present in the particular seal.

- Clearance, cl.

It is the radial clearance of the seal constriction

- Pitch, s.

It is the distance measured between the identical locations of two consecutive teeth or blades of the seal.

- Tooth Height, h.

It is the height of the tooth tip measured from its base

- Tooth Tip Thickness, t

It is the thickness of the seal tooth measured at the tip. It is also called the knife edge thickness.

- Diameter of the fins, D

It is the diameter of the labyrinth seals measured at the tip of rotor tooth.

Figure 2 illustrates the AEN sealing system of turbine stator-rotor cavities. The stator vanes of the turbine are mounted on an inner shroud ring. In order to control the leakage flow across the shrouds and to protect the disc outer diameter from hot gases, the shroud clearance is sealed with compressed air using turbine vane cooling air.

The supply of sealing air is in two-fold:

- The main part of sealing air is fed from the lower region of the cavity through equally spaced holes drilled in the vane shroud-ring and inclined to the vertical (holes do not impart any tangential component to the sealing air) (Figure 2 – [a]).
- The other part comes through the fir-tree of upstream rotating stage (Figure 2 – [b]).

Secondary air flow from the external bleed lines passes across the vane towards the seal-ring at inner platform. A part of this air is used for vane cooling and joins the gas flow path. The rest of the air is fed to the AEN seal through a set of holes drilled on the inner shroud ring. It is noted that the temperature of sealing air, after passing through the vane, is higher than that at the extraction point.

The AEN seal links the upstream and downstream cavities by effective sealing. The pressure difference across labyrinth seal, radial clearance and the seal cavity length (s minus t referred to figure 1) define primarily the amount of sealing air to the downstream cavity. The seal teeth on rotor are straight whereas that on stator are designed as helicoids. This design method reduces the accidental contact zone between rotating and stationary fins. Anyways the spiral angle of helicoids shape of stator teeth is very little, so the effect on leakage flow is considered negligible and the experiments can be done by means of a simplified 2D plane model.

The different seal pitches between rotor and stator facilitate the contact at different circumferential zone and, in this way, the abrasion and loss of efficiency are minimized.

The experiments described in the following sections have been carried out on a rig representing a scaled model of the third turbine vane sealing system.

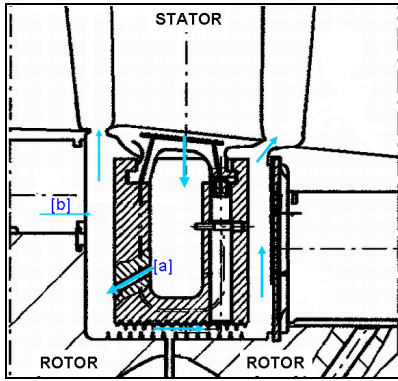


Fig. 2: Sealing system of 3rd turbine stage stator-rotor cavities

1.2 Preliminary analysis of rotational effects

Most studies show that there is a negligible effect of rotation on the leakage rate and heat transfer in labyrinth seals for the same seal clearance ([1], [3]). In most of the tests including rotational effects, the centrifugal growth and the thermal expansion were not measured and in some cases, they were considered theoretically. A significant variation of differential growth of rotor and stator from the cold stationary clearance will often result in significant uncertainties in the calculated characteristic values. The rotational effect can be described by the ratio of Taylor number to axial Reynolds number. Based on the measured rotational effects on the labyrinth flow and heat transfer, the rotation cannot be neglected at low axial Reynolds numbers and high Taylor numbers, [1].

These dimensionless numbers are defined as

$$Ta = \frac{2 \cdot u \cdot cl}{\nu} \sqrt{\frac{2 \cdot cl}{D}} \quad (1) \quad Re = \frac{2 \cdot m}{\mu \cdot \pi \cdot D} \quad (2)$$

Referring to AEN machine's operating conditions, the ratio Ta/Re is very low (~ 0.05). Experimental studies of Waschka et al. [1] point out that the effects of rotation play an important role (relevant reduction of the leakage rate and increase of the heat transfer) for Ta/Re ratio higher than approximately 0.2. In such way it can be assumed that the effects of rotation are negligible with regards to the AEN seal's operating conditions.

In order to confirm the last statement, CFD calculation has been performed. The simulated domain reproduce an actual test rig portion and the numerical boundary conditions have been imposed coherently with the actual AEN machine's operating conditions. The calculations have been performed using the commercial code ANSYS-CFX 12, while ICEM CFD has been used to generate a tetrahedral cell mesh. Compressibility effects have been taken into account and *High Resolution* advection schemes have been used. The fluid has been modeled as ideal gas and the properties of specific heat capacity, thermal conductivity and viscosity have been assumed as constants. Energy equation has been solved in terms of total temperature and viscous heating effects have been accounted for. The $k-\epsilon$ turbulence model, in its formulation made available by the CFD solver, has been used in conjunction with a high Reynolds approach.

Simulation convergence has been monitored through Navier Stokes equations residual (RMS residual $< 10^{-8}$).

Figure 3 shows simulation results at inlet Reynolds equal to 8000 for $S_{rot}/cl=9.8$. The rotation of rotor seal side generates radial pressure gradient that modifies principal flow field. This radial pressure gradient deforms flow path lines, in this way the seal behaviour seems to interlocking labyrinth seal. This analysis shows the rotational effect is higher if the mass flow rate is low and is related with the flux acceleration in tangential direction that occurs in the first seal tooth.

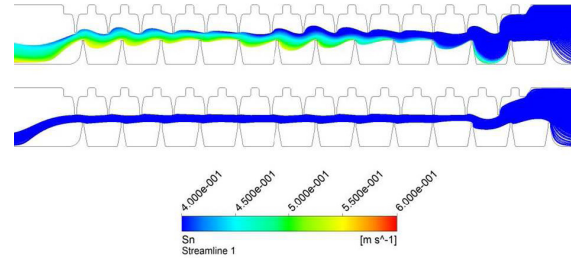


Fig. 3: $S_{rot}/cl=9.8$; $Re=8000$. Streamlines: rotating seal, top; fixed seal, bottom.

As the pressure ratio of the actual AEN's seals ranges from 1.4 to 1.6, figure 4 confirms that rotation effects could be assumed as negligible since the leakage mass flow rate changes of 7% within the whole range of seal's operating conditions. Further CFD analyses will be the subject of a successive publication.

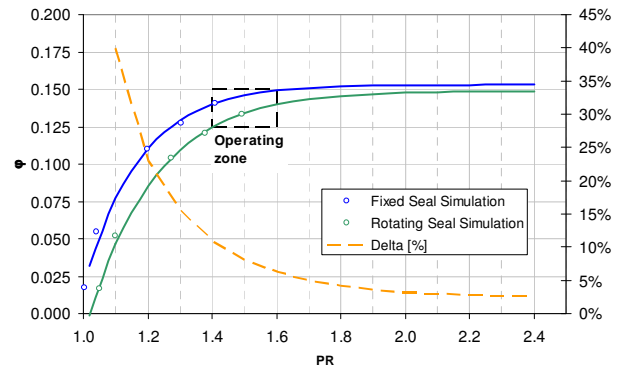


Fig. 4: $S_{rot}/cl=9.8$. CFD numerical comparison between rotating and fixed seals.

2.0 EXPERIMENTAL APPARATUS

The experiments make use of thermo-chromic liquid crystal (TLC) on the test surfaces in the presence of a cold/heated air stream to determine leakage flows and the local surface heat transfer coefficient.

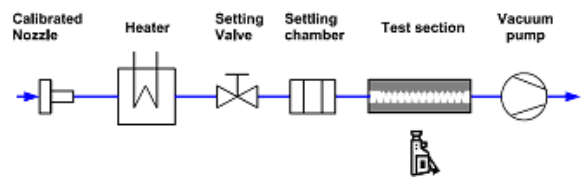


Fig. 5: Apparatus schematic

Figure 5 shows a schematic of the test apparatus. The rig consists of an open-loop suction type wind tunnel, which allows heat transfer and pressure loss measurements on several geometries. The mainstream air, at atmospheric pressure and ambient temperature, is metered through a calibrated nozzle and supplied to a 24.0 kW electronically controlled electric heater, where desired temperature is reached and kept constant. The air flow, before entering the PolyMethyl-MethAcrylate model, passes through a setting valve. Four rotary vane vacuum pumps (total power installed 59.0 kW) provide the suction for a maximum mass flow rate of 0.50 kg/s.

Figure 6 shows a cross section view of the seal model indicating the positions of pressure taps and thermocouples.

A pressure scanner Scanivalve® DSA 3217 with temperature compensated piezoresistive relative pressure sensors allow the measurement of total or static pressure in 16 different locations with an accuracy of 6.9 Pa.

With regard to temperature measurements, several T-type thermocouples, which results in an uncertainty of ± 0.5 K, are connected to a data acquisition/switch unit (HP/Agilent R 34970A); an external reference junction has been employed. Two thermocouples (located at position 1 and 16 of figure 6), mounted perpendicular to the flow, acquire mainstream recovery temperature. The thermocouples recovery factor, measured by means of a calibration test, has been evaluated as 0.68 and it has then been employed for the evaluation of air total temperature, T_0 , and static temperature, T .

A detailed error analysis yielded values of the uncertainty in the measurement of the gas mass flow was below 8%. Results deviated less than 4 percent from different sets of data which were acquired over a period of several months.

Based on a one-dimensional error analysis the maximum uncertainty of the local Nusselt numbers was computed to be in the range 12-25 percent.

The rig for this contactless seal (used in the third stator well of Ansaldo AE94.3A gas turbine) was designed 3 times scaled-up, in order to assure the same non dimensional parameters of the engine conditions. The width of the test section (400 mm) was selected in order to guarantee a spatial uniformity of axial velocity field.

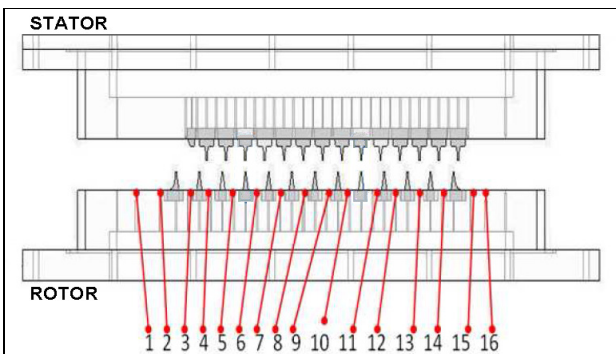


Fig. 6: labyrinth seal geometry and probe position

Figure 7 shows a view of the seal model indicating measuring locations in the inlet and outlet sections. In order to allow optical

access for the heat transfer measurements, the labyrinth geometry of the real engine was scaled up by a factor of three. The flow direction was always from the left to the right. This seal configuration presents two different tooth pitches. The upper side represents the stator geometry of the seal with 14 teeth and tooth pitch - tip thickness ratio $S_{sta}/t= 16.4$; while the lower side is the rotor one, with 13 teeth and tooth pitch - tip thickness ratio $S_{rot}/t= 19.6$.

In the experiments, the overall pressure ratio PR has been varied from 1 to 0.32 and Reynolds number Re from 4300 to 74500, which were selected close to engine operating condition values.

Five seal clearance configurations were investigated in order to analyze its influence on operating characteristics of the investigated seal geometry, as reported in table 1.

For all tested cases the axial relative position between stator and rotor teeth is the same. However preliminary tests showed, for any clearances, that the relative position has no effect on leakage flow rate. The reason of this behavior is that, for all possible relative axial positions, seal teeth with minimum gap are ever 2.

	S_{rot}/cl
Configuration 1	2.7
Configuration 2	4.9
Configuration 3	6.5
Configuration 4	9.8
Configuration 5	19.6

Table 1: test configurations

For heat transfer measurements the test is started by switching on the electric heater, and the resulting conduction of heat into the test section walls has been numerically simulated by a finite element code using specified heat transfer coefficients of the magnitude and spatial variation expected for the experiments. For these conditions together with physical properties for acrylic plastic, the simulations show that the depth of heating into the wall over the expected test duration is less than the wall thickness. In addition, lateral conduction in the wall has a negligible effect on the local surface temperature response. Details of data reduction used for this analysis have been given by Metzger and Bunker [20].

In the experiments here described, air temperature is determined from the inlet thermocouple measurement. The variation with time is recorded and approximated by steps, and the resulting superposed solution is solved for the local surface heat transfer coefficients, using observed local green peak times.

For leakage flow analysis, upstream and downstream pressure values were measured in order to calculate the pressure ratio PR. The inlet total values were calculated starting from static values using the isentropic equations:

$$\frac{T_0}{T} = 1 + \frac{\gamma - 1}{2} M^2 \quad (3)$$

$$\frac{P_0}{P} = \left(1 + \frac{\gamma-1}{2} M^2\right)^{\frac{\gamma}{\gamma-1}} \quad (4)$$

Where the inlet Mach value is calculated as

$$M = \frac{c}{\sqrt{\gamma R T}} \quad (5)$$

Where:

$$c = \frac{\dot{m}}{\rho \cdot B \cdot (h_{sta} + cl + h_{rot})} \quad (6) \quad \rho = \frac{P}{RT} \quad (7)$$

The static pressure in the outlet section plenum is used in place of pressure tap 16 (Figure 6), because the jet exiting the last two teeth may create a vortex (Figure 3) and a local decreasing of static pressure, which make this measurement not usable for data reduction

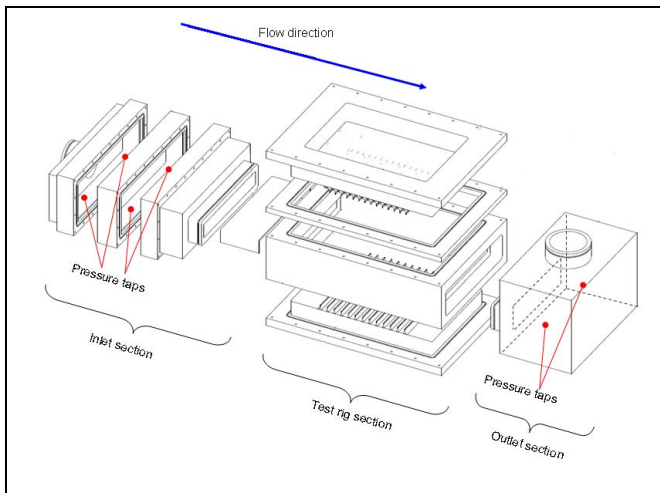


Fig. 7: test rig section

3.0 EXPERIMENTAL RESULTS

3.1 Leakage flow analysis

The influence of seal clearance on leakage flow will be presented in this section. For any given configurations, the leakage flow by changing the overall pressure ratio was tested. The flow function is well defined for each configuration. Reproducibility tests give a very small scattering.

In figure 8 the flow parameter, ϕ , for different pressure ratio is plotted in order to analyze the influence of S/cl parameter on the efficiency of the seal. It is needed to refer to the flow parameter, ϕ , in order to analyze the efficiency of the seal:

$$\phi = \frac{m\sqrt{RT_0}}{AP_0} \quad (8)$$

Using that definition (8), it is possible to understand how the seal is working for unity of geometrical area calculated as

$$A = B \cdot cl \quad (9)$$

All data reductions were made using the minimum geometrical area.

Figure 8 shows the flow parameter, of this kind of seal geometry, is no monotonic dependent with the clearance. In fact, a decreasing of seal clearance produces a decrease of the flow parameter (the seal efficiency increases) with a minimum for configuration 3, corresponding to the clearance in hot running condition in the engine.

Then a different behaviour is observed with an increase of the flow parameter for configuration 4 and 5 respectively. The flow behaviour for configuration 5 and 1 are very similar.

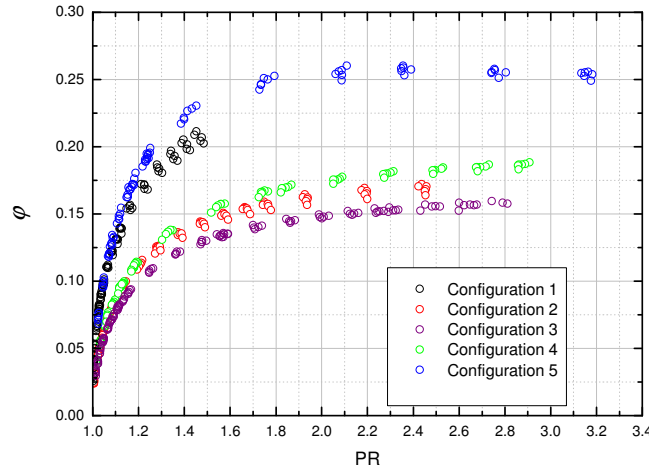


Fig. 8: Flow parameter versus overall pressure ratio

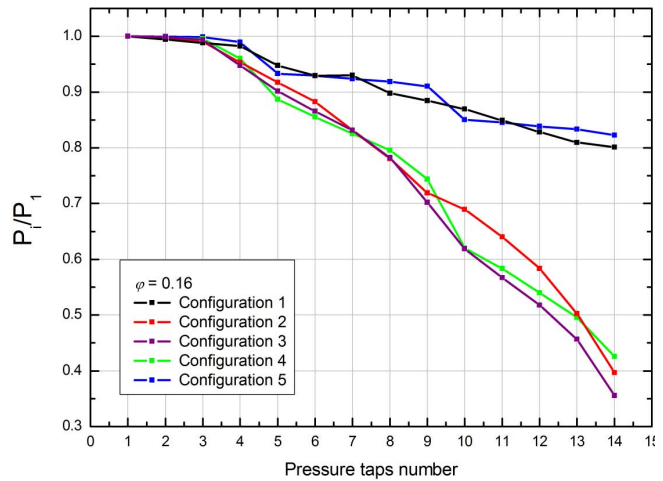


Fig. 9: pressure distribution for $\phi=0.16$

A different behaviour of the seal for different clearance is confirmed from the pressure distribution, as shown in figure 9 at fixed flow parameter $\phi=0.16$. The pressure gradients for configuration 1 are almost constant along the cavity. Hence, the presence of tooth on both side with different pitch can be assimilate to a distributed pressure loss (turbolated channel).

A similar behaviour was obtained for the configuration 2 and 3. In these cases the loss factor is higher than for

configuration 1 with consequently higher overall pressure ratio. The pressure drops rise along the seal due to the higher velocity. Although a similar overall pressure ratio is observed for configuration 4, the pressure loss system is quite different. A lower seal clearance makes more visible the presence of 2 points where a minimum geometrical area is present. A higher pressure loss belongs to these points. Vice versa the rest of the seal shows a lower pressure ratio.

This behaviour is more pronounced with configuration 5. The entire pressure ratio is due to the tooth 4 and 9. The pressure losses produced by the rest of the tooth are very small.

This is clearer in Figure 10 where the pressure ratio between each tooth is plotted for this configuration as example.

The 65% of overall pressure loss is concentrated in two teeth and only 35% belongs to others.

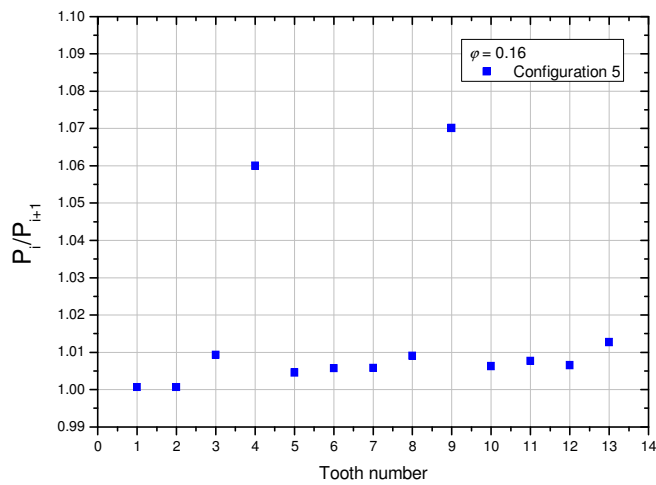


Fig. 10: Configuration 5; $\phi=0.16$: pressure ratio of each tooth

3.1 Heat transfer Analysis

The small influence of seal clearance on both local and overall heat transfer coefficient will be presented in this section. Three Reynolds number was tested for all configurations.

The hydraulic diameter of the labyrinth gap ($2 \cdot cl$) represents the characteristic length scale for the Reynolds number and Nusselt number defined as:

$$Re_{rig} = \frac{2 \cdot m}{\mu \cdot B} \quad (10) \quad Nu = \frac{htc \cdot 2 \cdot cl}{k} \quad (11)$$

The viscosity and conductivity were assumed to be constant during tests. Only for flat wall between the teeth of rotor side, a 1D conductive heat transfer can be assumed. Thus results only for this region will be presented. The reference gas temperature for the local heat transfer coefficients is assumed to vary linearly between the inlet and outlet static temperatures (position 1 and 16 of figure 6).

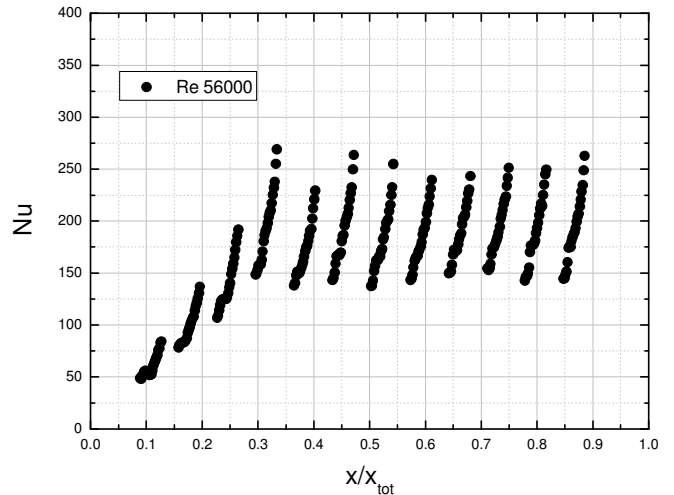


Fig. 11: Configuration 1; $Re_{rig}=56000$: Nusselt distribution

The heat transfer coefficient at the seal inlet is constant and assumes a value compared with that provided by classical correlations for flows within rectangular ducts. For example, using the common correlation for long ducts provided by the Dittus-Boelter:

$$Nu = 0.023 \times Re_{rig}^{0.8} \times Pr^{1/3} \quad (12)$$

an error of 3% is obtained for Reynolds number of 56000 with a maximum error of 7% for all cases. This result allows us to validate the experimental apparatus and post processing method.

Figure 11 shows that between two teeth an increase in heat transfer coefficient is observed in the stream wise direction due to the recirculation that sets in downstream each tooth.

The qualitative distribution of the local Nusselt numbers exhibits an increase moving forward due to the presence of tooth that breaks the boundary layer producing a high turbulence level. Starting from the 4-th teeth, which is the first constriction with minimum effective area, a more stable distribution of heat transfer coefficient was obtained. It means that starting from this point subsequent constriction can't produce further increase in turbulence level. Small variations are shown depending on the relative position of stator and rotor teeth.

In figure 12 the effect of Reynolds number can be observed for configuration 1. The values of the local Nusselt numbers increase with increasing Reynolds number as expected from literature review. The qualitative distribution exhibits no definite dependence on Reynolds number.

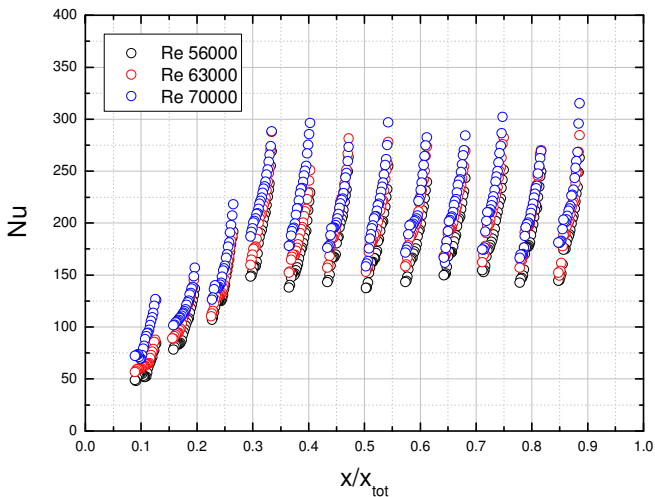


Fig. 12: Configuration 1: Nusselt distribution

The small dependence on Reynolds number (Re_{rig}) is confirmed for all configurations as shown in figure 13 and 14 for configuration 2 and 4. Whereas a dependence on the gap width is clear for local Nusselt number. When the clearance decreases, the effects related to the presence of teeth on stator side is more marked in the local Nusselt number distribution on rotor side as shown in figure 14.

Note that these considerations are valid for the stationary rig; however, according to Waschka et al. [1], the rotation has a negligible effect also on the heat transfer for low values of Ta/Re ratio, as it occurs in AEN engine conditions. Since analysis Waschka et al. [1], is referred to straight thought seal, CFD investigation of heat transfer in rotating conditions is planned for our seal configuration.

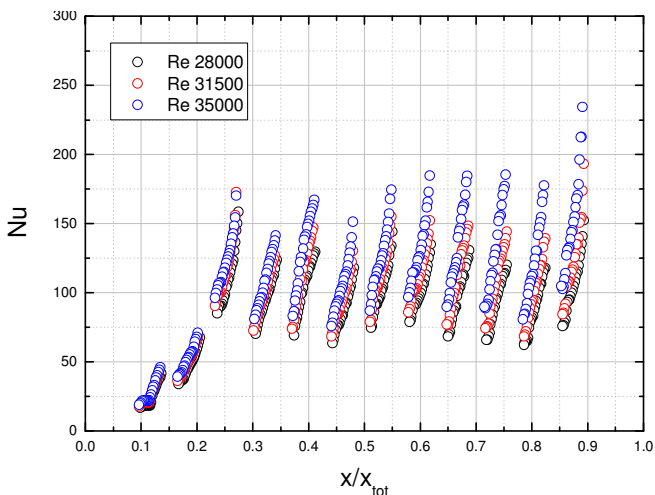


Fig. 13: Configuration 2: Nusselt distribution

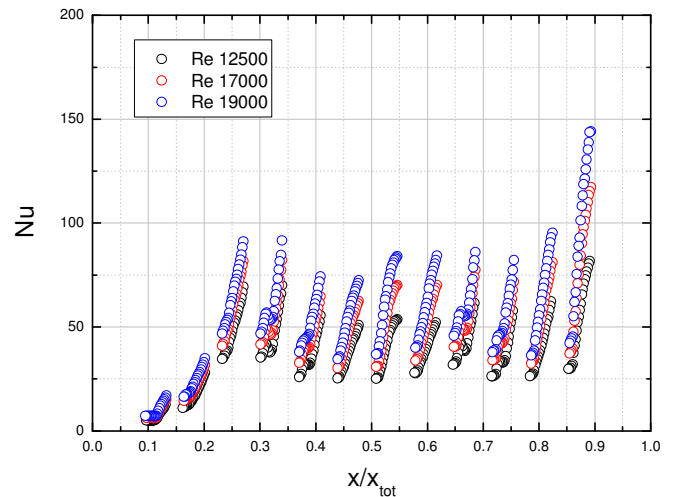


Fig. 14: Configuration 4: Nusselt distribution

5.0 LEAKAGE MODELS APPLICATION

Leakage flow through labyrinth seals is generally modeled as sequential series of throttlings through the narrow blade tip clearance. Ideally, the kinetic energy increasing across each annular orifice would be completely dissipated in the downstream cavity. However, the dissipation is not complete. Various researchers handle this in different ways. Gamal [7] discussed all existing leakage models in his dissertation.

For labyrinth seals, the energy dissipation is achieved by a series of constrictions and cavities. When the fluid flows through the constriction (under each tooth), a part of the pressure energy is converted into kinetic energy, which is dissipated through small scale turbulence – viscosity interaction in the cavity that follows. Therefore, equations to predict the leakage flow rate can be developed by comparing the seal to a series of orifices and cavities. Using this analogy, the mass flow rate is modeled as a function of the flow coefficient factor under each tooth and the carry-over coefficient, which accounts for the turbulent dissipation of kinetic energy in a cavity.

Martin presented the first leakage equation in which the leakage flow rate is modeled basing on the work done to achieve the required pressure drop.

The ideal labyrinth flow functions imply one dynamic head pressure loss downstream of each fin. The carry-over factor should account for the effect that only a fraction of the dynamic head is lost, i.e. some dynamic head is carried over.

For data reduction several models have been considered: Hodkinson and Vermes appeared better to describe phenomena of the studied labyrinth seal.

Hodkinson's model is the modification of Egli's Equation. Whereas Egli used an empirical coefficient to account for kinetic energy carry-over, Hodkinson [12] developed a semi-empirical expression for this coefficient based on an assumption regarding the gas jet's geometry.

He assumed that the fluid jet expands conically from the tip of the upstream tooth at a small angle, β . A part of the jet impinges on the downstream tooth to recirculate in the cavity, dissipating the kinetic energy associated with it, while a portion of the jet travels under the downstream tooth and carries over the kinetic energy to the next cavity. He assumed the angle β to be a function of seal geometry only.

Vermes' [23] developed his own kinetic energy carry-over factor expression and combined with Martin's leakage equation. Vermes' carry-over factor was developed from boundary layer theory. He introduced the residual energy factor, α , in order to account for the residual energy in the flow as it passes from one stage to the next one.

One selected the two models data reduction has been carried out using the equation 13.

$$\frac{m\sqrt{RT_0}}{P_0AK} = F_{co} \sqrt{\frac{1 - \left(\frac{P_{out}}{P_{0,in}}\right)^2}{N - \ln\left(\frac{P_{out}}{P_{0,in}}\right)}} \quad (13)$$

As well known, the previous equation was derived based on the following assumptions:

- The gas reasonably modelled using isothermal flow with constant values of pressure and density at each cavity of the seal.
- The validity of the gas law maintained.

Since, the experimental data, available at present, are not sufficient to deduce an exact empirical expression of the kinetic carry-over factor, thus, the expressions of kinetic energy carry-over factor from standard leakage models have been used. Hokinson's and Vermes' empirical expressions were used (Table2). Both methods modelled kinetic carry-over factor coefficient as a function of seal geometry.

In our case, seal tooth heights and pitches are different for stator and rotor sides. Because the experiments were performed varying only the clearances, as geometrical parameter, to calculate carry over factor, average spacing and height are used.

	Hodkinson's model	Vermes' model
Carry-over factor	$K = \frac{1}{\sqrt{1 - \left(\frac{N-1}{N}\right) \left(\frac{c}{s-t}\right) \left(\frac{c}{s-t} + 0.02\right)}}$	$K = \sqrt{\frac{1}{1 - \alpha}}$
Residual energy factor		$\alpha = \frac{8.52}{\frac{s-t}{c} + 7.23}$

Table 2: Applied leakage models

A computer program was developed, which helps in getting a pressure dependent flow coefficient factor from the experiment data using the discharge coefficient method and the pressure dependent flow function:

$$F_{co} = \frac{m \cdot \sqrt{R \cdot T_0}}{A \cdot P_0} \cdot K \cdot \sqrt{\frac{1 - \left(\frac{P_{out}}{P_{0,in}}\right)^2}{N - \ln\left(\frac{P_{out}}{P_{0,in}}\right)}} \quad (14)$$

These pressure dependent data are used to get the coefficients fitting the flow coefficient factor. Then, the flow coefficient factor is expressed as an exponential function of pressure ratio as below:

$$F_{co} = a_0 + a_1 \cdot \exp\left(-a_2 \cdot \frac{P_{0,in}}{P_{out}}\right) \quad (15)$$

Both literature models show a good agreement with experimental data. Figures 15 and 16 show, respectively, the comparison between experimental and numerical mass flow rate and model's error. With reference with pressure taps in figure 6, figures 17, 18 and 19 show the pressure distribution across seal cavities for all geometrical configurations, for three values of pressure ratio.

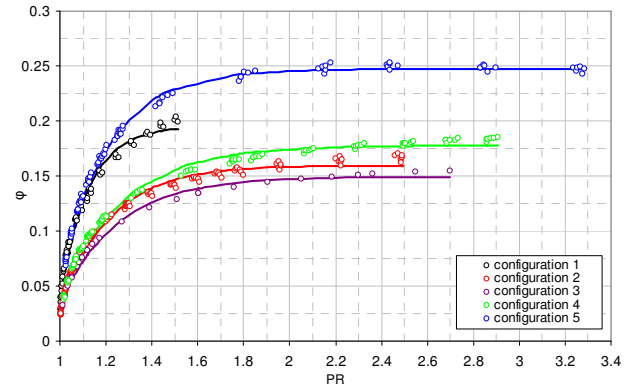


Fig. 15: comparison between experimental and numerical flow parameter

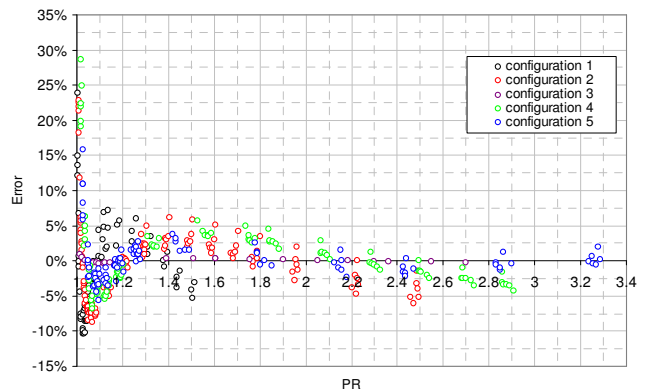


Fig. 16: model error for flow parameter

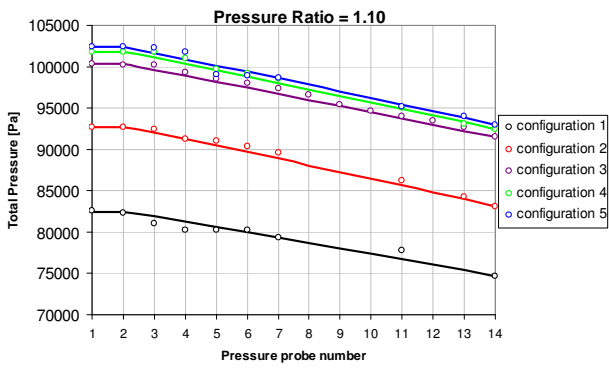


Fig. 17: Seal cavity pressure distribution for PR=1.10

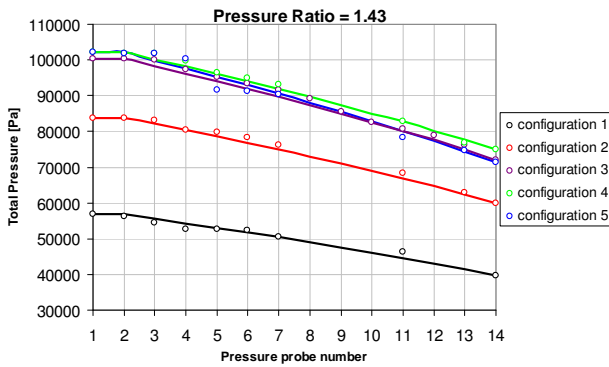


Fig. 18: Seal cavity pressure distribution for PR=1.43

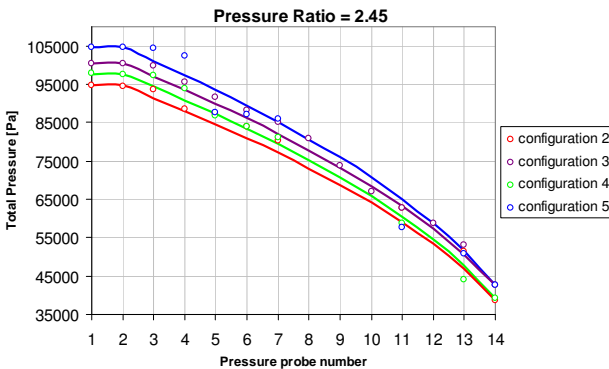


Fig. 19: Seal cavity pressure distribution for PR=2.45

Results of flow coefficient factor calculated by means of the two methods highlights the following points/observations:

1. The difference between two results of flow coefficient factor depends on the different models to calculate carry-over factor;
2. The minimum value of flow coefficient factor, for all values of pressure ratio, corresponds to the clearance in hot running conditions (Figure 20 and Figure 22);
3. The seal behaviour is almost independent from pressure ratio (Figure 21 and Figure 23).

The agreement with experimental data is similar for both models because in the mass flow rate formula (13), appears the

product of carry-over factor and flow coefficient factor, and this value derives from experimental data.

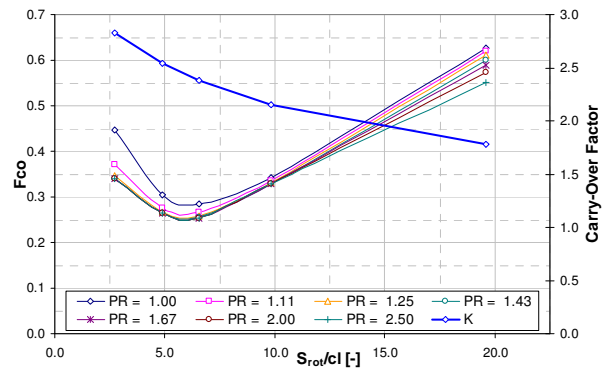


Fig. 20: Flow coefficient factor calculated with Hodkinson's model vs. S_{rot}/cl

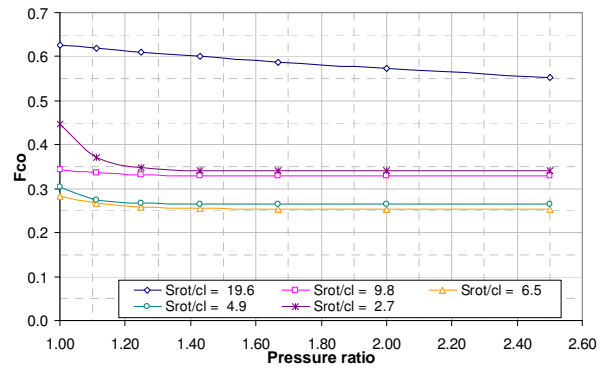


Fig. 21: Flow coefficient factor calculated with Hodkinson's model vs. Pressure ratio

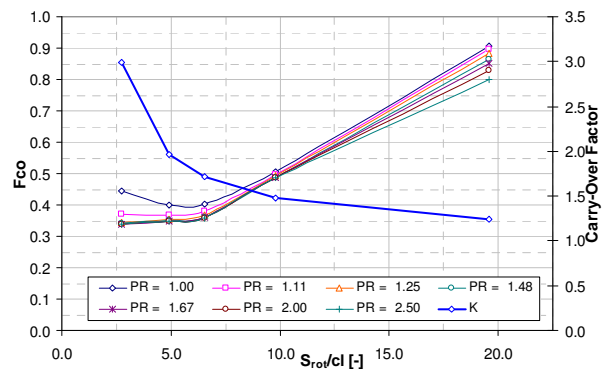


Fig. 22: Flow coefficient factor calculated with Verme's model vs. S_{rot}/cl

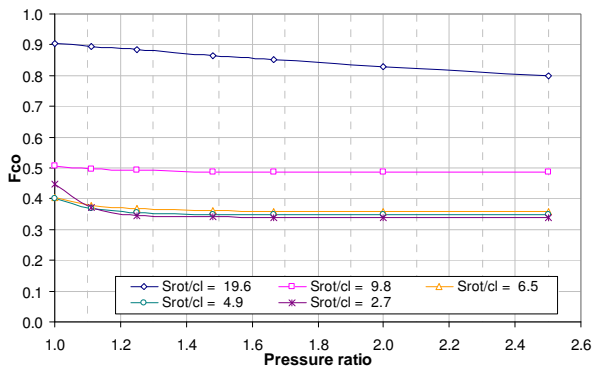


Fig. 23: Flow coefficient factor calculated with Vermes's model vs. Pressure ratio

6.0 SUMMARY

Measurements of the leakage rate and the heat transfer were performed on a scaled-up stationary rig of a contactless seal used in heavy-duty gas turbines.

Results of experiments carried out for five values of clearances, show that the flow parameter of this type of seal geometry is not monotonic dependent with the clearance. This behaviour assures lower leakage flow dependence on clearance than straight through configuration and, thus, makes such type of seals preferable for gas turbine applications.

Tests showed, for any clearances, that the relative position between stator and rotor teeth has no effect on leakage flow rate. The reason of this behavior is that, for all possible relative axial positions, seal teeth with minimum gap are ever 2. A lower seal clearance makes more visible the presence of these 2 points where a minimum geometrical area is present. A higher pressure loss is associated to these points. Vice versa the rest of the seal shows a lower pressure ratio.

On the other hand, the heat transfer analysis showed the values of the local Nusselt number that increases with increasing Reynolds number, as expected from literature review. When the clearance decreases, the effects related to the presence of teeth on both stator and rotor side is more marked in the local Nusselt number distribution.

For data reduction several models have been considered: Hodkinson and Vermes appeared better to describe phenomena of the studied labyrinth seal. These approaches show a good agreement with experimental data.

The future work will consist of in more deeply experiments in order to define carry over factor correlation specific for AEN seal geometry.

Moreover, by means of CFD and rig tests, additional research effort will be done in order to study the effect of rotation in particular on the heat transfer (since the test rig is stationary).

7.0 NOMENCLATURE

A	flow section	[m ²]
AEN	Ansaldo Energia	[-]
B	width test rig	[m]
c	rig axial flow velocity	[m/s]
cl	seal clearance	[m]
D	seal diameter	[m]
Fco	Flow coefficient factor	[-]
h	tooth height	[m]
htc	heat transfer coefficient	[W/m ² K]
k	air conductivity	[W/m K]
K	Carry-over factor	[-]
M	axial Mach number	[-]
m	mass flow rate	[kg/s]
N	seal number	[-]
P	static pressure	[Pa]
P ₀	total pressure	[Pa]
PR	pressure ratio	[-]
R	Specific gas constant	[J/kg K]
s	seal pitch	[m]
T	static temperature	[K]
t	tooth tip thickness	[m]
T ₀	total temperature [K]	
u	cavity peripheral velocity	[m/s]
x	rig axial length	[m]
x _{tot}	total rig axial length	[m]

Greek letters:

α	residual energy factor	[-]
γ	ratio of specific heat	[-]
μ	dynamic viscosity	[kg/s m]
ν	cinematic viscosity	[m ² /s]
ρ	air density	[kg/m ³]
φ	flow parameter	[-]

Subscripts:

<i>o</i>	total condition
<i>In</i>	inlet condition
<i>Out</i>	outlet condition
<i>Rot</i>	rotor
<i>Sta</i>	stator

Adimensional group:

Nu	Nusselt Number
Pr	Prandtl Number
Re	Axial Reynolds Number
Re _{rig}	Rig Reynolds number
Ta	Taylor Number

8.0 REFERENCES

- [1] Waschka, W., Witting, S., Kim, S., 1992, "Influence of High Rotational speeds on the heat transfer and discharge coefficients in labyrinth seals". ASME Journal of Turbomachinery vol.114:462-468
- [2] Kutz, K. J., Speer, T. M., 1994, "Simulation of the secondary air system of aero engines" Transactions of the ASME vol.116
- [3] Zimmermann, H., Wolff, K. H., 1998, "Air System Correlations – Part 1: Labyrinth Seals" ASME Paper No. 98-GT-206
- [4] Bonzani, F., Bozzi, L., Mantero, M., Vinci, A., Innocenti, L., Micio, M., 2010 "1D tool for stator-rotor cavities integrated into a fluid network solver of heavy-duty gas turbine secondary air system" ASME Paper No. GT2010-22203
- [5] Reichert, W. A., Janssen, M., 1996, "Cooling and sealing air system in industrial gas turbine engines" ASME Paper No. 96-GT-256
- [6] Denecke, J., Faber, J., Dullenkopf, K., Bauer, H. J., 2005 "Dimensional analysis and scaling of rotating seals" ASME paper No. GT2005-68676
- [7] Metzger, D. E., Bunker, R. S., 1985, "Heat Transfer for Flow Through Simulated Labyrinth Seals", Symposium on Transport Phenomena in Rotating Machinery, Honolulu, USA
- [8] Myer Kutz, 1998, "Mechanical Engineers' Handbook", 2nd Edition, John Wiley & Sons, Inc.
- [9] Ahmed Mohamed Gamal Eldin, 2007, "Leakage and Rotordynamic Effects of Pocket Damper Seals and See-Through Labyrinth Seals", A Doctoral Dissertation, Texas A&M University.
- [10] Venard, J. K., and Street, R. L., 1982, "Elementary Fluid Mechanics", John Wiley & Sons, New York.
- [11] General Electric., 1973, "Labyrinth Seals", Duct Systems, Fluid Flow Division, Section 405.7
- [12] Dereli, Y, and Eser, D., 2004, "Flow Calculations in Straight-Through Labyrinth Seals by Using Moody's Friction-Factor Model", Association for Scientific Research, Mathematical and computational applications, 9(3), pp. 435-442.
- [13] Yucel, U. and Kazakia, J.Y., 2001 (January), "Analytical Prediction Techniques for Axisymmetric Flow in Gas Labyrinth Seals", Technical Brief, Journal of Engineering for Gas Turbines and Power, 123, pp. 255-257.
- [14] Stocker, H.L., Cox, D.M., and Holle, G.F., 1977, "Aerodynamic Performance of Conventional and Advanced Design Labyrinth Seals with Solid-Smooth, Abradable, and Honeycomb Lands", NASA CR-135307
- [15] Saikishan Suryanarayanan, 2009, "Labyrinth Seal Leakage Equation", A Thesis for Master of Science, Texas A&M University.
- [16] Willenborg, K., Kim, S., and Wittig, S. 2001. Effects of Reynolds Number and pressure ratio on leakage loss and heat transfer in a stepped labyrinth seal. ASME Journal of Turbomachinery 123:815-822.
- [17] Wittig, S., Dorr, L., and Kim, S. 1983. Scaling effects on leakage losses in labyrinth seals. ASME Journal of Engineering for Power 105:305-309.
- [18] Poling B. E., Prausnitz J. M., O'Connell J. P., 2001. "The properties of gases and liquids". McGraw-Hill International Editions.
- [19] Egli, A., 1935, "The Leakage of Steam through Labyrinth Seals", Transactions of the ASME, 57, pp.115-122.
- [20] Metzger, D. E., and Bunker, R. S., 1985. "Heat transfer for flow through simulated labyrinth seals". presented at the Symposium on Transport Phenomena in Rotating Machinery, Honolulu, USA.
- [21] Willenborg, K., Kim, S., and Wittig, S., 2001. "Effect of reynolds number and pressure ratio on leakage loss and heat transfer in a stepped labyrinth seal". ASME J. Turbomach., 123, pp. pp 815–822.
- [22] Willenborg, K., Schramm, V., Kim, S., and Wittig, S., 2002. "Influence of a honeycomb facing on the heat transfer in a stepped labyrinth seal". ASME J. Eng. Gas Turbines Power, 124, pp. pp 133–139.
- [23] Vermes, G., 1961 (April), "A Fluid Mechanics approach to the Labyrinth Seal Leakage Problem", ASME Transactions – Journal Engineering for Power, 83 (2), pp. 161-169.

ACKNOWLEDGEMENTS

The authors would like to acknowledge the help of Mr Muniappan Selvakumar for his technical support during writing of this article.